α-Glucosidase Inhibitory Activity and Cytotoxicity of CeO₂ Nanoparticles Fabricated Using a Mixture of Different Cerium Precursors

Shaidatul Najihah Matussin, Fazlurrahman Khan, Pathum Chandika, Mohammad Hilni Harunsani, Norhayati Ahmad, Young-Mog Kim, Won-Kyo Jung, and Mohammad Mansoob Khan*

Read Online

ACCESS | Metrics & More | Article Recommendations | SI Supporting Information

ABSTRACT: A mixture of three distinct cerium precursors (Ce(NO$_3$)$_3$·6H$_2$O, CeCl$_3$·7H$_2$O, and Ce(CH$_3$COO)$_3$·H$_2$O) was used to prepare cerium oxide nanoparticles (CeO$_2$ NPs) in a polyol-mediated synthesis. Different ratios of diethylene glycol (DEG) and H$_2$O were utilized in the synthesis. The properties of the synthesized CeO$_2$ NPs, such as structural and morphological properties, were investigated to observe the effect of the mixed cerium precursors. Crystallite sizes of 7−8 nm were obtained for all samples, and all synthesized samples were confirmed to be in the cubic phase. The average particle sizes of the spherical CeO$_2$ were between 9 and 13 nm. The successful synthesis of CeO$_2$ can also be confirmed via the vibrational band of Ce−O from the FTIR. Antidiabetic properties of the synthesized CeO$_2$ NPs were investigated using α-glucosidase enzyme inhibition assay, and the concentration of the synthesized CeO$_2$ NPs was varied in the study. The biocompatibility properties of the synthesized CeO$_2$ NPs were investigated via cytotoxicity tests, and it was found that all synthesized materials showed no cytotoxic properties at lower concentrations (62.5−125 μg/mL).
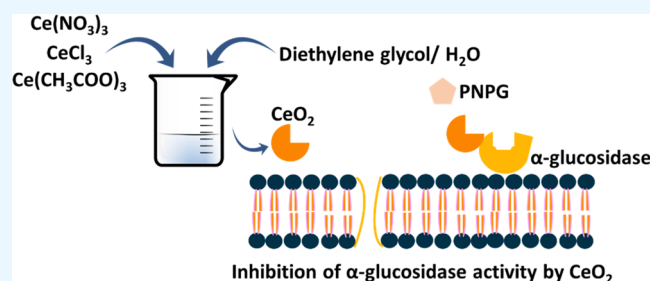
1. INTRODUCTION

Polyols such as ethylene glycol, diethylene glycol, triethylene glycol, etc. have been used in the polyol-mediated synthesis of metal nanoparticles (NPs), such as Co, Cu, and Pt, metal oxides NPs, and metal ligands complexes.[1] Generally, polyol can be used as a solvent and a reducing agent. It can also attach to the surface of formed nanomaterials and influence its particle size and morphology.[1] Moreover, due to the chelating properties of polyols, which compensate for their lower polarity, the behavior of metal salts in polyol and water is quite similar.[2] Their low toxicity and high biodegradability show that polyols can be considered green solvents.[2] Furthermore, additional benefits of polyols include their scalability and application in continuous-flow synthesis, the fact that the reductive properties of polyols allow for the rapid formation of elemental metals, and the ease with which polyols may be easily removed from the particle surface following synthesis. All of these advantages make polyols an attractive choice for a variety of applications.[2]

Among the rare earth metal oxides, cerium oxide (CeO$_2$) has attracted much attention.[3,4] Owing to its redox capabilities (Ce^{4+}/Ce^{3+}), it is classified as one of the most reactive rare earth oxides, despite the fact that it is an n-type semiconductor with a broad band gap (3.2 eV).[5−7] CeO$_2$ has been utilized for a wide variety of applications, ranging from those connected to the environment, energy, and biomedicine.[8−12] CeO$_2$ NPs, nanowires, and nanotubes have been synthesized by various methods,

for instance, solvothermal, spray pyrolysis, hydrothermal, sonochemical reactions, and precipitation.[13−16] Furthermore, CeO$_2$ has been synthesized using the polyol method; for example, Cheng et al. reported on a polyol-mediated approach to synthesize CeO$_2$.[17] The authors used a solvothermal method with a polyol/ethanol mixed solvent as the reaction medium. The synthesized CeO$_2$ showed wrinkled spherical morphology with an average size of 2 μm. In another study, Xin et al. reported on the synthesis of monodispersed CeO$_2$-based quantum dots (QDs) that were prepared by heating triethylene glycol and Ce precursor salts together.[18] The prepared CeO$_2$-based QDs possessed uniform particle sizes of less than 5 nm. In addition, the function of counteranion in the precursors of metal salts has not been subjected to significant research on nanomaterials. It has been suggested that the anions might be selectively adsorbed on the facets, which would affect the morphological and structural characteristics of the synthesized materials.[19,20]
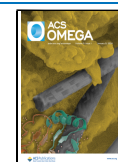
CeO$_2$ NPs have especially gained attention as they exhibit an enormous range of applications in the biomedical area.[10,21] So far, biomedical studies on diagnosing and treating life-threatening diseases using CeO$_2$ have shown potentially good performance.[21] For instance, one study reported on the α-glucosidase inhibitory activity using plant extract-mediated CeO$_2$.[22] The synthesized CeO$_2$ successfully inhibited 31.28% of the α-glucosidase enzyme. This shows that CeO$_2$ has the potential to inhibit the α-glucosidase enzyme, and its inhibition can be achieved more by tuning the properties of CeO$_2$ such as their structure and morphology.[23] Diabetes mellitus has been recognized as one of the major life-threatening diseases in the world. Increased blood glucose levels, which may result in significant consequences such as cardiovascular disease, nephropathy, and neuropathy, are a distinguishing feature of diabetes mellitus type II (T2DM).[24] One of the therapeutic approaches to controlling postprandial hyperglycemia, which refers to the abnormality of glucose homeostasis in T2DM, is by hindering the digestion of dietary carbohydrates. Dietary carbohydrates will be broken down by pancreatic α-amylase into simple monosaccharides in the digestive system.[25] This is followed by the degradation of the monosaccharides to glucose by α-glucosidase, in which glucose finally enters the bloodstream by absorption.[26,27] As a result, maintaining postprandial blood glucose levels under control is essential, and this may be accomplished by researching and developing novel therapeutic drugs. It is important to note that inhibiting the digestive enzyme α-glucosidase is beneficial in treating type II diabetes because it delays glucose absorption in the small intestine and enables a more regulated absorption.[23]

Our research team has just recently published a paper on the synthesis of CeO$_2$ NPs utilizing three distinct types of cerium precursors, as well as an investigation into the α-glucosidase inhibitory capabilities and cytotoxicity of the generated CeO$_2$ NPs.[28] Each CeO$_2$ NP synthesized using Ce(NO$_3$)$_3$·6H$_2$O, CeCl$_3$·7H$_2$O, and Ce(CH$_3$COO)$_3$·H$_2$O precursors showed different properties, α-glucosidase inhibitory capabilities, and cytotoxicity, suggesting there were some effects of different cerium precursors.[28] However, to the best of our knowledge, there are no reports on the synthesis of CeO$_2$ using a mixture of different cerium precursors. Therefore, this study is an extension of the recently reported work.[28] This work reported on the synthesis of CeO$_2$ NPs using a mixture of different cerium precursors, whereas in the previous work, the synthesis of CeO$_2$ was carried out using different cerium precursors separately. Aside from that, various proportions of diethylene glycol (DEG) and water were used in the fabrication of the NPs. The impact of mixed cerium precursors and varied DEG/H$_2$O ratios on the structural and morphological features of the synthesized CeO$_2$ was examined in this study. In conclusion, the various produced CeO$_2$ NPs were assessed for their biological activities, namely, their ability to inhibit the α-glucosidase enzyme and their cytotoxic effects.

2. EXPERIMENTAL METHODS

2.1. Chemicals Used. For the synthesis of CeO$_2$ NPs, cerium(III) nitrate hexahydrate (Ce(NO$_3$)$_3$·6H$_2$O, 99%), cerium(III) chloride heptahydrate (CeCl$_3$·7H$_2$O, 99%), and cerium acetate hydrate (Ce(CH$_3$COO)$_3$·H$_2$O, 99%) were obtained from Sigma-Aldrich. Commercial CeO$_2$ (C-com) used for comparison was obtained from Sigma-Aldrich. Diethylene glycol (C$_4$H$_{10}$O$_3$, 99%) as a solvent in the synthesis was purchased from Alfa-Aesar. Double-distilled water that has

been purified (Aquatron, England) was used throughout the experiment. α-Glucosidase ($\geq$50 units/mg protein), 4-nitro-phenyl α-D-glucopyranose (PNPG, C$_{12}$H$_{15}$NO$_8$, 99%), acarbose (C$_{25}$H$_{43}$NO$_{18}$, $\geq$95%), sodium carbonate (Na$_2$CO$_3$, $\geq$99.5%), sodium phosphate monobasic monohydrate (NaHPO$_4$·H$_2$O, $\geq$99%), and sodium phosphate dibasic heptahydrate (Na$_2$HPO$_4$·7H$_2$O) were all obtained from Sigma-Aldrich for the α-glucosidase inhibitory study. RAW 264.7 cell lines (mouse macrophage) were purchased from the American Type Culture Collection (ATCC, Rockville, MD) for the cytotoxicity investigation. Sigma-Aldrich supplied the cytotoxicity assays penicillin, streptomycin, fetal bovine serum (FBS), dimethyl sulfoxide, and MTT (3,4,5-dimethylthiazol-2-yl)-2−5-diphenyl tetrazolium bromide.

2.2. Synthesis of CeO$_2$ Nanoparticles. CeO$_2$ NPs were prepared via polyol-mediated synthesis by mixing three different cerium precursors, namely, Ce(NO$_3$)$_3$·6H$_2$O, CeCl$_3$·7H$_2$O, and Ce(CH$_3$COO)$_3$·H$_2$O, in a different DEG/H$_2$O ratio solution. In the synthesis, several ratios of DEG to H$_2$O were used, including 0/25, 5/20, 10/15, 15/10, 20/5, and 25/0 mL, with a total volume of 25 mL (Figure S1). Exactly 0.05 M of the cerium precursor solution was prepared in which the three cerium precursors were mixed in a way that one-third of 0.05 M of the solution was made up of each cerium precursor. The mixture was heated gradually to 80 °C after being stirred at room temperature for 5 min. After that, 4 mL of a 1 M NaOH solution was added slowly. The solution was heated to 100 °C for 4 h while being agitated to encourage the formation of white precipitates. The CeO$_2$ precipitate took the form of a gel. The product was then rinsed three times in water and centrifuged at 3500 rpm. Following final purification, the material was calcined for 2 h at 600 °C before being milled into powder CeO$_2$ NPs. The DEG/H$_2$O ratio, in this case, 0/25, 5/20, 10/15, 15/10, 20/5, and 25/0 mL, is represented by the CMx coding for this batch of CeO$_2$ (Table S1).

2.3. Instrumentations. X-ray diffraction (XRD) with Cu Kα radiation (λ = 1.5418 Å) was used to identify the crystal phase of CMx NPs by using Shimadzu XRD-7000. Vibrational bands related to DEG and NP formation were identified using FT-IR (Shimadzu IRPrestige-21 Fourier Transform Infrared Spectrophotometer) at room temperature in the 400−4300 cm^{-1} range. Field emission transmission electron microscopy (FE-TEM, JEM-F200, JEOL Ltd., Tokyo, Japan) was used to examine the morphology and selected area electron diffraction (SAED) of the CMx NPs. Kratos Analytical's AXIS Nova was used for the X-ray photoelectron spectroscopy (XPS) of CMx NPs. A UV−vis spectrophotometer (Shimadzu UV 1900, Japan) was used to evaluate the absorbance of the enzyme−substrate solution for α-glucosidase inhibition activity. A microplate reader (Gen 5TM ELISA Bio Tek, Winooski, VT) was used to detect absorbance at 540 nm for the cell cytotoxicity investigation.

2.4. Inhibition of α-Glucosidase Enzyme Activity. The α-glucosidase inhibitory activity of CMx NPs was measured using a conventional technique with minor modifications and was tested in triplicates.[29] In the experiment, a centrifuge tube with a capacity of 1.5 mL was utilized, and varied quantities of CMx NPs (0.5, 1.5, and 2.5 mg) were placed in the tube. Using a vortex, 250 μL of 1 M phosphate buffer solution (PBS, pH 6.8) was combined in the tube before 250 μL of 1.5 U/mL α-glucosidase (enzyme). It was then incubated at 37 °C for 10 min. After incubation, 250 μL of 0.5 mM p-nitrophenyl-α-D-glucopyranoside (PNPG, substrate) was added to the reaction
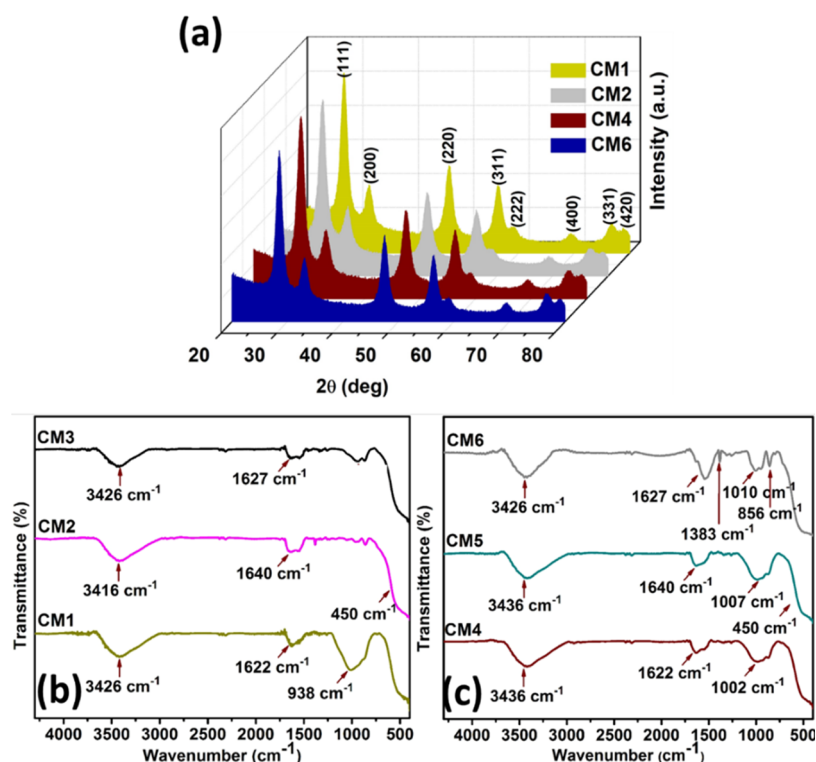
Figure 1. (a) XRD patterns and (b, c) FTIR spectra of CMx NPs synthesized by using a mixture of three different cerium precursors.

Table 1. Calculated Crystallite Size as well as the Lattice Properties, Cell Volumes, and Peak Ratio of the CMx NPs

sample	average crystallite size (nm)	lattice parameter, (a, (Å))	volume (a^3 (Å^3))	ratio between 1st and 2nd peaks
CM1	7.39	5.371	154.94	3.63
CM2	7.05	5.390	156.59	3.98
CM4	7.39	5.341	152.36	4.23
CM6	8.22	5.429	160.01	4.12

solution. The mixture was then put back into the incubator for an additional 30 min at 30 °C. After adding 1 mL of a sodium carbonate solution with a concentration of 0.2 M to complete the reaction, the mixture was centrifuged, and the absorbance of the solution was determined at a wavelength of 405 nm.

2.5. Cytotoxicity Test. The MTT assay was used to determine whether CMx NPs exhibited cytotoxicity *in vitro* when tested against murine macrophage cell line RAW 264.7. The macrophage cells were grown in Dulbecco's minimal Eagle's medium, which also included 100 U/mL penicillin, 100 mg/mL streptomycin, and 10% fetal bovine serum. The temperature was maintained at 37 °C, and 5% of carbon dioxide was present in the air. After the cells had been trypsinized, they were grown in 96-well plates and treated with various doses of CMx NPs for a period of 24 h. To analyze the cytotoxicity study, the culture media were changed out for a new medium that was freshly prepared and included MTT at a concentration of 1 mg/mL. This was followed by an incubation period of 4 h. After that, the crystals of formazan in each well were dissolved by adding 100 μL of dimethyl sulfoxide. To get an accurate reading of the absorbance, a microplate reader was used. The experiment was carried out three times to ensure accuracy.

3. RESULTS AND DISCUSSION

A mixture of $Ce(NO_3)_3 \cdot 6H_2O$, $CeCl_3 \cdot 7H_2O$, and $Ce(CH_3COO)_3 \cdot H_2O$ was used to produce CeO_2 NPs using the polyol synthesis technique, abbreviated as CMx. In this study,

codes CM1-CM6 indicate the amount of DEG used in the synthesis (0, 5, 10, 15, 20, and 25 mL, respectively).

3.1. X-ray Diffraction Analysis. Figure 1a shows the XRD patterns of cubic-phase CeO_2, which confirms the successful synthesis of CeO_2 using a mixture of all three cerium precursors: $Ce(NO_3)_3 \cdot 6H_2O$, $CeCl_3 \cdot 7H_2O$, and $Ce(CH_3COO)_3 \cdot H_2O$. As the XRD patterns did not show any additional peaks, this indicates that there were no contaminants or other phases of CeO_2 that developed. Therefore, the materials that were synthesized are pure. In addition, the influence of the DEG/H_2O ratio on the structural characteristics of the CMx NPs may be seen by predicting their average crystallite sizes using the Debye−Scherrer formula. This allows one to see how the ratio affects the NPs (1):[30]

$$D = k\lambda/\beta \cos\theta \qquad (1)$$

where λ stands for the wavelength of the X-ray, θ denotes Bragg's angle, and β is the full width at half-maximum of the distinctive peaks.

The average crystallite size from CM1 to CM6 was increased slightly from 7.39 to 8.22 nm. However, CM4 shows a crystallite size similar to CM1. Overall, this might suggest that a higher amount of DEG NPs has an effect on the average crystallite size of CeO_2, and in the case of CM1 and CM4, the effect of 5 and 15 mL DEG is somewhat similar. Furthermore, the lattice parameters of CMx NPs were observed to be similar, except for CM4. The cell volume in the range of 152.36−160.01 Å^3 was
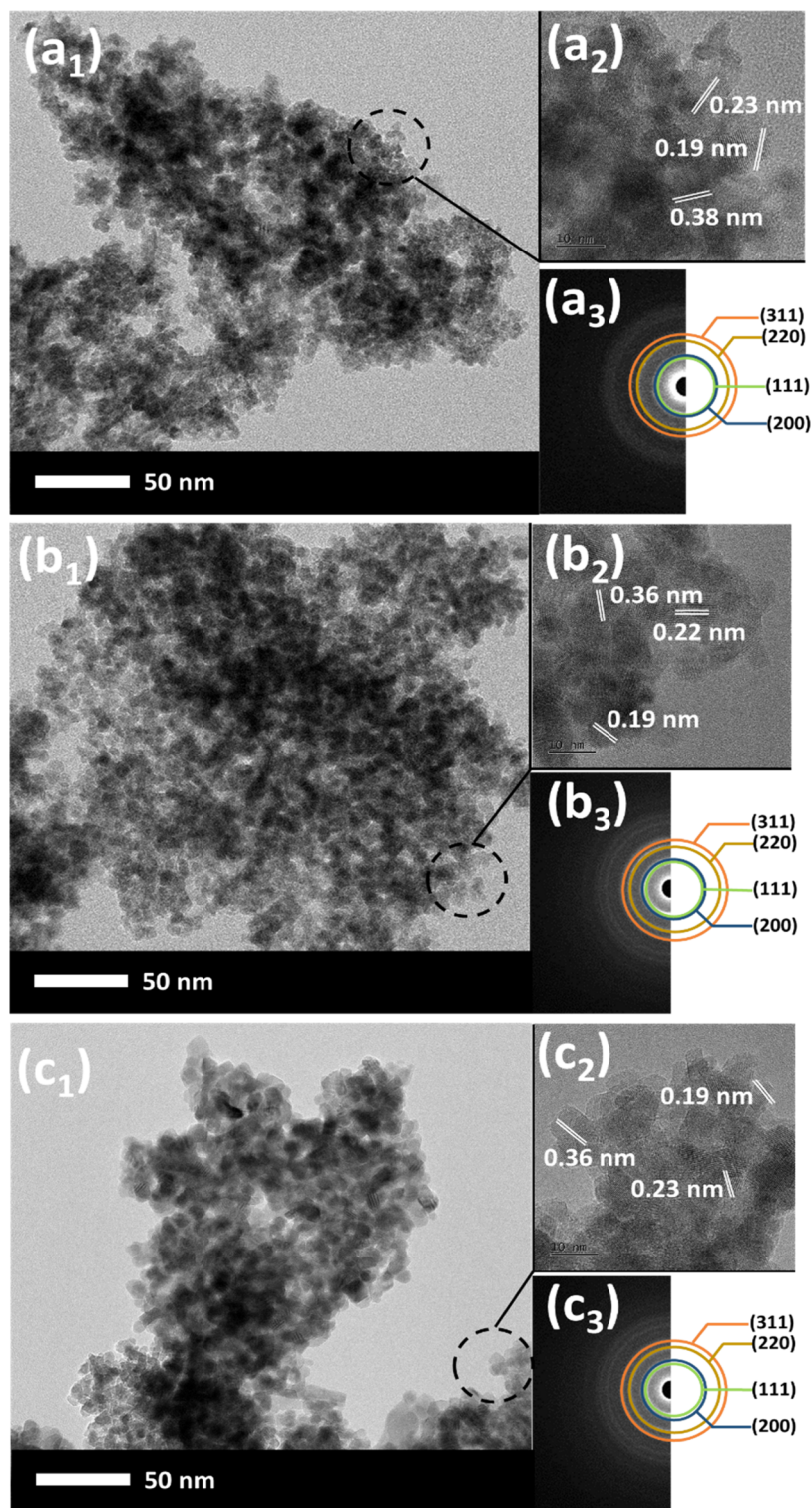
Figure 2. (a_1-c_1) TEM, (a_2-c_2) HRTEM, and (a_3-c_3) SAED pattern of (a) CM1, (b) CM4, and (c) CM6.

observed using different DEG/H_2O ratios. The combined effect of NO_3^-, Cl^-, and CH_3COO^- anions might not be seen from the XRD, but the variation in the crystallite size that was observed might be due to the amount of DEG used (Figure 1a and Table 1).

The effect of DEG on the crystallite size of the CMx NPs can be seen in Figure 1a and Table 1. When 0 mL of DEG was used to synthesize CM1, the crystallite size was about 7.39 nm. However, as the amount of DEG increased, the crystallite size

increased slightly. It was found that the average crystallite size increased with the addition of DEG. The oxygen groups in diethylene glycol molecule might interact with Ce^{4+} ions to mediate the synthesis of CMx NPs.[31]

3.2. Fourier Transform Infrared Spectroscopy. At room temperature, FTIR analysis of CMx samples was carried out in the 400−4300 cm^{-1} region. The FT-IR spectra of CeO_2 in CMx are shown in Figure 1b,c, respectively. In brief, the bands correspond to C−O stretching at a frequency of 1100−1000
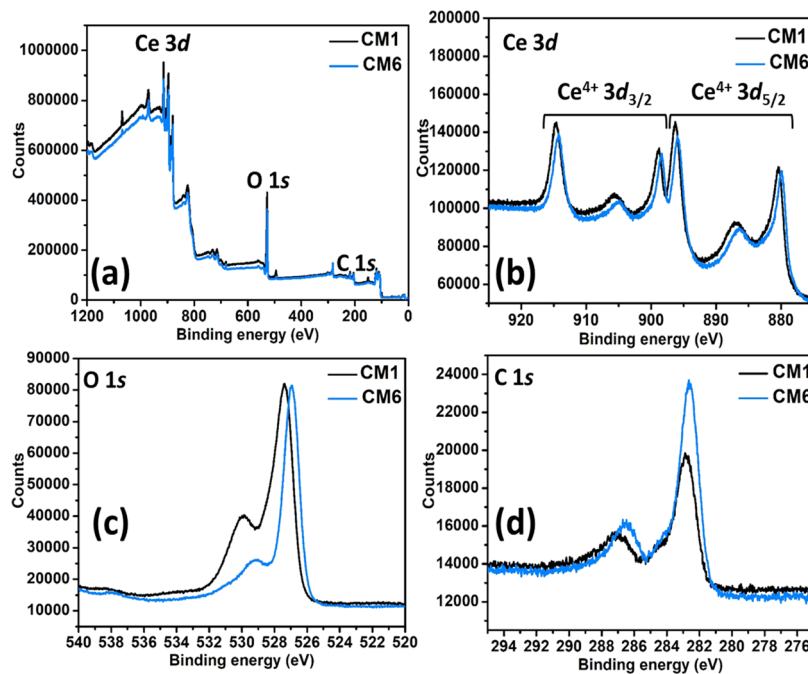
Figure 3. XPS spectra of CM1 and CM6 NPs: (a) Survey scan; (b) Ce 3d, (c) O 1s, and (d) C 1s.

cm^{-1}, C−H bending at a frequency of 1350 cm^{-1}, O−C=O stretching at a frequency of 1600 cm^{-1}, and O−H stretching at a frequency of 3300 cm^{-1}. It is interesting to note that increasing the amount of DEG in the CeO_2 NPs decreased the amount of C−O stretching. In spite of the different DEG/H_2O ratios, it was discovered that the O−H stretching vibrations occurred at a frequency of around 3390 cm^{-1} and that their intensities were comparable. On the other hand, the C−H bending at a frequency of around 1310 cm^{-1} became more pronounced; the presence of acetate ions may have brought this on.[32] It is possible that nitrate residues are responsible for the peak that appears between 800 and 900 cm^{-1} in some of the samples.[32]

3.3. Transmission Electron Microscopy. The influence of a number of different ratios of DEG/H_2O was detected in relation to the size and shape of the CeO_2 NPs. Figure 2 displays the TEM of CeO_2 that were produced by combining Ce(NO$_3$)$_3$·6H$_2$O, CeCl$_3$·7H$_2$O, and Ce(CH$_3$COO)$_3$·H$_2$O. The TEM picture of the CM1 NPs that were produced at a ratio of 0/25 mL of DEG/H_2O is shown in Figure 2a$_1$. CeO_2 NPs that were produced have a size distribution that is not uniform and are averaged 13 nm in diameter. From the previous study, CeO_2 NPs synthesized separately using Ce(NO$_3$)$_3$·6H$_2$O, CeCl$_3$·7H$_2$O, and Ce(CH$_3$COO)$_3$·H$_2$O showed larger average particle size, i.e., 28, 34, and 29 nm, respectively, at the same DEG/H_2O ratio.[28] This shows that mixing the three distinct cerium precursors might lead to a smaller particle size. As can be seen in Figure 2a$_2$, the d-spacing values of the lattice planes were obtained using HR-TEM images. The d-spacing values are predicted to be around 0.38, 0.23, and 0.19 nm which correspond to the (111), (200), and (220) planes, respectively.[33] In addition, the diffraction pattern of CM1 NPs is analyzed by selected area electron diffraction (SAED), which reveals that the fluorite cubic CeO_2 structure shows four wide rings (Figure 2a$_3$), which can be ascribed to the (111), (200), (220), and (311) reflections. Figure SII provides a view of the unprocessed photographs of the SAED patterns.

The spherical morphology became more significant with 15/10 mL of DEG/H_2O ratio, as shown by CM4 NPs in Figure 2b$_1$. The average size of the particles was found to be 12 nm, indicating that the particle size has been marginally reduced. Figure 2b$_2$ displays the HR-TEM images that were used to determine the d-spacing values of the lattice planes. The values were determined to be about 0.36, 0.22, and 0.19 nm correspond to the (111), (200), and (220) planes, respectively.[33] Moreover, Figure 2b$_3$ exhibits the SAED of CM4, which is attributed to the (111), (200), (220), and (311) planes.

The TEM picture of CM6 is shown in Figure 2c$_1$. The morphology of the particles remained unchanged after treatment with 100% DEG. In addition to this, the particle size was seen to be somewhat reduced, coming in at around 9 nm. From previous work, at the same DEG/H_2O ratio, CeO_2 NPs that were synthesized using different Ce precursors, Ce(NO$_3$)$_3$·6H$_2$O, CeCl$_3$·7H$_2$O, and Ce(CH$_3$COO)$_3$·H$_2$O, and showed larger particle sizes at around 16, 28, and 20 nm, respectively.[28] Therefore, it can be said that a mixture of cerium precursors might reduce the particle size. The determination of the d-spacing values of the lattice planes was done and found to be around 0.36, 0.23, and 0.19 nm (Figure 2c$_2$), which corresponds to the (111), (200), and (220) planes, respectively. Furthermore, the SAED displays four different rings (Figure 2c$_3$), which are assigned to the (111), (200), (220), and (311) planes.[33] Therefore, the effect of a mixture of three different precursors can be seen in the suppression of particle growth. From CM1 to CM6, the particle size decreased only decreased slightly. This might also be due to DEG acting as a capping agent in the synthesis. DEG and the three cerium precursors greatly control both the morphology and size.

3.4. X-ray Photoelectron Spectroscopy. Only two samples, CM1 and CM6, were selected for XPS examination. Figure 3 displays the XPS spectra of both CM1 and CM6, respectively. As can be seen in Figure 3a, the survey scan reveals the presence of Ce 3d, O 1s, and C 1s. Figure 3b depicts six typical Ce 3d peaks in both CM1 and CM6. In the XPS spectrum

of CM1, Ce^{4+} $3d_{3/2}$ is responsible for the three peaks located at the higher binding energy (898.72, 905.82, and 914.42 eV), while Ce^{4+} $3d_{5/2}$ is responsible for the other three peaks located at the lower binding energy (880.51, 886.82, and 898.09 eV).[34] Similarly, the peaks for CM6 that are located at 898.50, 904.72, and 914.22 eV are ascribed to Ce^{4+} $3d_{3/2}$, while the other three peaks that are situated at 879.86, 886.39, and 895.89 eV are attributable to Ce^{4+} $3d_{5/2}$.

The XPS spectra of O 1s can be shown in Figure 3c, and it can be seen that both CM1 and CM6 display two asymmetrical peaks. This indicates that there are OH^-, O^{2-}, and O^- atoms present on the surfaces of the nanostructures. It has been observed that the peak with the greater binding energy is related to O^{2-} vacancies and adsorbed ^-OH, while the peak with the lower binding energy is attributed to the metal−oxygen binding.[34,35] Figure 3d provides a representation of the C 1s XPS spectrum, which may have been caused by the DEG coating on the surface of CeO_2. Because all of the DEG was used in the synthesis of CM6, it has a higher carbon content. Table 2 contains information on the atomic concentrations of C 1s, O 1s, and Ce 3d.

Table 2. Atomic Concentration (%) of Ce 3d, O 1s, and C 1s in CM1 and CM6

sample	atomic concentration (%)		
	Ce 3d	O 1s	C 1s
CM1	21.2	60.6	18.2
CM6	23.6	47.8	28.6

4. APPLICATIONS

4.1. INHIBITION OF α-GLUCOSIDASE ACTIVITY

The α-glucosidase inhibitory property of the CMx NPs was investigated to establish whether CMx NPs could prevent the enzyme α-glucosidase from performing its normal function. By catalyzing the conversion of oligosaccharides and disaccharides into monosaccharides, the α-glucosidase enzyme plays a role in the metabolic process responsible for the breakdown of carbohydrates.[36] As a result, inhibiting the activity of α-glucosidase might cause a delay in the digestion and absorption of carbohydrates, which contributes to a decrease in blood glucose levels.[37] The potential of CMx NPs to suppress α-glucosidase enzyme activity was evaluated using a dose range of 0.5 to 1.5 mg/mL of the compound. As a positive control,

acarbose was used, and the α-glucosidase inhibition employing C-com was also evaluated and compared with that of artificially produced CeO_2.

Figure 4a depicts the α-glucosidase inhibition activity of the CMx samples. The absorbance of the enzyme−substrate solution was measured at 405 nm, and the α-glucosidase inhibition activities in % were calculated using the equation below (2):[38]

$$\% \text{ inhibition} = \frac{(\text{Abs}_b - \text{Abs}_s)}{\text{Abs}_b} \times 100 \qquad (2)$$

where Abs_b represents the absorbance of the blank solution (one that does not include any CeO_2) and Abs_s represents the absorbance of the final solution containing CeO_2 NPs.

Based on the findings, C-com showed the lowest activity compared with the synthesized materials. CM5 produced the highest α-glucosidase inhibition activity at the highest concentration (2.5 mg/mL), followed by CM6 and CM4. At 1.5 mg/mL, CM4 showed the highest % inhibition activity, followed by CM5 and CM6 (Table SII). The behavior of these materials might be due to the particle size and shapes possessed by CM4, CM5, and CM6, i.e., spherical particles with particle size between 9 and 13 nm, which might affect the active site of the enzyme.[23]

At 0.5 mg/mL, CM1, CM2, CM3, CM4, CM5, and CM6 showed inhibition percentages of 39.92 ± 3.23, 38.73 ± 1.88, 35.78 ± 3.15, 39.70 ± 3.54, 38.08 ± 3.40, and 39.36 ± 3.79%, respectively. The efficiency of inhibition activity of the samples can be observed as such: CM1 > CM4 > CM6 > CM2 > CM5 > CM3. However, at the highest dosage, i.e., 2.5 mg/mL, CM6 showed slightly better activity among the samples which was then followed by CM5 and CM4, respectively. On the other hand, CM2 and CM3 showed decreased α-glucosidase inhibition activities at both 1.5 and 2.5 mg/mL. The optimum concentration of the synthesized CeO_2 NPs can be said to be at 0.5 mg/mL. It can also be said that CeO_2 NPs synthesized using more DEG showed better responses than the CeO_2 NPs synthesized with lower DEG.

In general, the enzymatic reaction that occurs by α-glucosidase toward the PNPG substrate results in the formation of an enzyme−substrate complex. This complex is responsible for the breakdown of PNPG into more manageable molecules. As a consequence of this, the amount of glucose in the blood will rise. The presence of an inhibitor may stop the formation of a complex between an enzyme and its substrate. Owing to their size, shape, and crystalline structure, NPs have the ability to
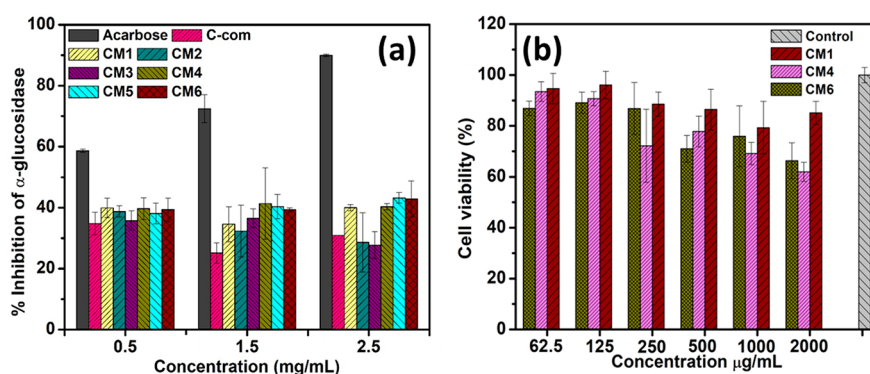

Figure 4. (a) α-Glucosidase inhibition activity using all of the CMx samples and (b) cell viability (cell cytotoxicity) (%) of CM1, CM4, and CM6 NPs.

enter the active site of an enzyme, where they may then compete with PNPG.[23] Figure 4a shows that the proportion of α-glucosidase inhibition for CMx NPs ranges between 30 and 40%. On the other hand, CMx NPs have the potential to modify the structure of the enzyme by attaching themselves to the active site of the enzyme via noncovalent bonding. Because of this, the development of an enzyme−substrate complex is prevented, and as a result, α-glucosidase inhibitory activity may be shown.[39,40] This could imply that CMx NPs are able to enter the active site of the enzyme or might indicate that the NPs are able to change the active site of the enzyme.

4.2. CYTOTOXICITY TEST

The MTT test was used to analyze the cytotoxicity of CMx NPs on RAW 264.7 macrophages in order to determine the biocompatibility of CeO_2 NPs that were manufactured for use in pharmaceutical applications. At concentrations of 62.5, 125, 250, and 500 μg/mL, none of the fabricated CeO_2 NPs exhibited any cytotoxic effects that were harmful to the cells (Figure 4b).

CM1 showed 94.69 ± 6.00 and 96.06 ± 5.40 cell viability at 62.5 and 125 μg/mL, respectively, but the cell viability decreased with increasing concentration, with about 85−75% cell viability at 250−1000 μg/mL. At 2000 μg/mL, the cell viability of CM1 was about 85.14 ± 4.51%, which is similar to its cell viability at 250 μg/mL, which is 86.47 ± 7.96%. This shows that increasing the concentration to more than 1000 μg/mL would not result in lower cell viability, as observed at 250 and 2000 μg/mL. On the other hand, CM4 demonstrated lower cell viability, which is 69.15 ± 4.34 and 61.93 ± 3.70% compared to the other NPs at higher concentrations (1000 and 2000 μg/mL), respectively. However, at the lower concentrations (62.5 and 125 μg/mL), CM4 showed higher cell viability than CM6, in which it showed 93.49 ± 3.87% and 90.74 ± 2.76%, respectively. This indicates that CM4 is not toxic to cells at low concentrations. CM6 showed over 80% cell viability at the lower concentrations (62.5−250 μg/mL), where the cell viability of CM6 was higher than CM4 at 250 μg/mL. At higher CM6 concentrations (500−2000 μg/mL), the cell viability was about 65−70%. Based on the observation, at the three lowest concentrations, i.e., 62.5−250 μg/mL, CM1 and CM6 showed high cell viability, whereas, in the case of CM4, it showed high cell viability at the two lowest concentrations only, i.e., 62.5 and 125 μg/mL. Overall, the results indicate that CM1 has shown the highest cell viability.

From the previous work, CN1 which was synthesized using $Ce(NO_3)_3\cdot 6H_2O$ and 0/25 (DEG/H_2O) ratio showed the highest cell viability at each concentration similar to CM1.[28] On the other hand, CC1 and CA1 which were prepared using $CeCl_3\cdot 7H_2O$ and $Ce(CH_3COO)_3\cdot H_2O$, respectively, with 0/25 (DEG/H_2O) ratio showed the decrease in cell viability especially at 2000 μg/mL. Individual CN1, CC1, and CA1 showed different cell viability in which when CeO_2 NPs were prepared by mixing three different precursors, it showed high cell viability. This means that the toxicity of the samples can be reduced by mixing Ce precursors.

The quantity of DEG used in the production of CeO_2 may have some bearing on the level of cytotoxicity shown by the CMx NPs. It has been found that DEG is biocompatible and has a low to moderate level of toxicity; however, the particle size and shapes of the produced NPs also have a significant effect in the level of cytotoxicity.[2,41,42] According to the literature, the toxicity rises as the particle size becomes smaller.[43,44] As a result of this finding, the study came to the conclusion that CM1 was

safe to use since it had an average particle size of 13 nm. As the particle size was reduced in CM4 and CM6, there was an accompanying increase in cytotoxicity. In addition, it has been shown that the poisonous effects of CMx are proportional to the concentration of the compound. On the other hand, it was found that the impact of dose varied from case to case. Because cell density influences the actual dosage of particles that are delivered to each cell, this may also be the cause of the effect that cell behavior has on cell density.[41] This impact could be easier to understand if the dosage was represented as a mass per cell number (μg/10^6 cells). In order to objectively quantify the particle−cell interaction and optimize dose compatibility, it is essential to take note of the mass of NPs as well as the quantity of NPs that were disseminated to the cell medium.[41]

5. CONCLUSIONS

Through a process known as polyol-mediated synthesis, CeO_2 NPs were produced by adjusting the ratio of diethylene glycol (DEG) to water and with a combination of three distinct cerium precursor salts. Variations in the DEG and H_2O ratios used in the synthesis were analyzed for their effects on the structural and morphological characteristics of the CeO_2 NPs that were manufactured. The results of the XRD study indicated that the typical size of a crystallite ranged from 7 to 8 nm. CeO_2 NPs with a spherical shape were measured to have an average particle size ranging from 9 to 13 nm. The use of FTIR allowed for the investigation of the presence of DEG molecules on the surface of the newly produced CeO_2 NPs. The α-glucosidase enzyme inhibition test was used to assess whether the newly produced CeO_2 NPs have any antidiabetic characteristics. CeO_2 NPs that were manufactured with a larger quantity of DEG had an α-glucosidase inhibition activity of around 40.0%. Furthermore, increasing the sample dose did not have a significant impact on the level of α-glucosidase inhibition activity shown by the CeO_2 NPs. The cytotoxicity tests were used in order to evaluate the biocompatibility qualities of the produced CeO_2 NPs. The results of these tests revealed that all of the synthesized materials were nontoxic at lower concentrations ranging from 62.5 to 125 μg/mL. Hence, the synthesized CeO_2 NPs are promising α-glucosidase inhibitors with high biocompatibility.

■ ASSOCIATED CONTENT

ⓢ Supporting Information

The Supporting Information is available free of charge at https://pubs.acs.org/doi/10.1021/acsomega.3c02524.

Schematic diagram for the polyol-mediated synthesis of CeO_2 (Figure SI); amount of diethylene glycol and water used to synthesize CM samples (Table SI); raw images of SAED pattern of CM1, CM4, and CM6 (Figure SII); and percentage inhibition of α-glucosidase activity using CM samples (Table SII) (PDF)

■ AUTHOR INFORMATION

Corresponding Author

Mohammad Mansoob Khan − Chemical Sciences, Faculty of Science, Universiti Brunei Darussalam, Gadong BE 1410, Brunei Darussalam; ● orcid.org/0000-0002-8633-7493; Email: mmansoobkhan@yahoo.com, mansoob.khan@ubd.edu.bn

Authors

Shaidatul Najihah Matussin − *Chemical Sciences, Faculty of Science, Universiti Brunei Darussalam, Gadong BE 1410, Brunei Darussalam*

Fazlurrahman Khan − *Institute of Fisheries Sciences, Pukyong National University, Busan 48513, Republic of Korea; Marine Integrated Biomedical Technology Center, The National Key Research Institutes in Universities and Research Center for Marine Integrated Bionics Technology, Pukyong National University, Busan 48513, Republic of Korea*

Pathum Chandika − *Marine Integrated Biomedical Technology Center, The National Key Research Institutes in Universities and Research Center for Marine Integrated Bionics Technology, Pukyong National University, Busan 48513, Republic of Korea*

Mohammad Hilni Harunsani − *Chemical Sciences, Faculty of Science, Universiti Brunei Darussalam, Gadong BE 1410, Brunei Darussalam*

Norhayati Ahmad − *Institute for Biodiversity and Environmental Research, Universiti Brunei Darussalam, Gadong BE 1410, Brunei Darussalam; Environmental and Life Sciences, Faculty of Science, Universiti Brunei Darussalam, Gadong BE 1410, Brunei Darussalam*

Young-Mog Kim − *Marine Integrated Biomedical Technology Center, The National Key Research Institutes in Universities, Research Center for Marine Integrated Bionics Technology, and Department of Food Science and Technology, Pukyong National University, Busan 48513, Republic of Korea;* ⬤ orcid.org/0000-0002-2465-8013

Won-Kyo Jung − *Marine Integrated Biomedical Technology Center, The National Key Research Institutes in Universities, Research Center for Marine Integrated Bionics Technology, and Major of Biomedical Engineering, Division of Smart Healthcare and New-Senior Healthcare Innovation Center (BK21 Plus), Pukyong National University, Busan 48513, Republic of Korea;* ⬤ orcid.org/0000-0002-1615-750X

Complete contact information is available at:
https://pubs.acs.org/10.1021/acsomega.3c02524

Author Contributions

S.N.M.: Methodology; investigation, data curation; writing—original draft. **F.K.**: Methodology, investigation, data curation, review, and editing. **P.C.**: Methodology, investigation, data curation, review, and editing **M.H.H.**: Supervision, writing—review and editing. **N.A.**: Supervision, writing—review and editing. **Y.-M.K.**: Resources, formal analysis. **W.-K.J.**: Resources, formal analysis. **M.M.K.**: Supervision, conceptualization, funding acquisition, writing—review and editing.

Notes

The authors declare no competing financial interest.

■ REFERENCES

(1) Teichert, J.; Doert, T.; Ruck, M. Mechanisms of the Polyol Reduction of Copper(Ii) Salts Depending on the Anion Type and Diol Chain Length. *Dalton Trans.* **2018**, *47* (39), 14085−14093.

(2) Dong, H.; Chen, Y. C.; Feldmann, C. Polyol Synthesis of Nanoparticles: Status and Options Regarding Metals, Oxides, Chalcogenides, and Non-Metal Elements. *Green Chem.* **2015**, *17* (8), 4107−4132.

(3) Khan, M. M.; Matussin, S. N. Sm_2O_3 and Sm_2O_3-Based Nanostructures for Photocatalysis, Sensors, CO Conversion, and Biological Applications. *Catal. Sci. Technol.* **2023**, *13*, 2274.

(4) Abdulwahab, K. O.; Khan, M. M.; Jennings, J. R. Doped Ceria Nanomaterials: Preparation, Properties, and Uses. *ACS Omega* **2023**, *8* (34), 30802−30823.

(5) Amoresi, R. A. C.; Oliveira, R. C.; Marana, N. L.; de Almeida, P. B.; Prata, P. S.; Zaghete, M. A.; Longo, E.; Sambrano, J. R.; Simões, A. Z. CeO2 Nanoparticle Morphologies and Their Corresponding Crystalline Planes for the Photocatalytic Degradation of Organic Pollutants. *ACS Appl. Nano Mater.* **2019**, *2* (10), 6513−6526.

(6) Matussin, S. N.; Harunsani, M. H.; Khan, M. M. CeO2 and CeO2-Based Nanomaterials for Photocatalytic, Antioxidant and Antimicrobial Activities. *J. Rare Earths* **2023**, *41* (2), 167−181.

(7) Matussin, S. N.; Khan, F.; Harunsani, M. H.; Kim, Y.-M.; Khan, M. M. Visible-Light-Induced Photocatalytic and Photoantibacterial Activities of Co-Doped CeO_2. *ACS Omega* **2023**, *8* (13), 11868−11879.

(8) Khan, M. E.; Khan, M. M.; Cho, M. H. Ce3+-Ion, Surface Oxygen Vacancy, and Visible Light-Induced Photocatalytic Dye Degradation and Photocapacitive Performance of CeO2-Graphene Nanostructures. *Sci. Rep.* **2017**, *7* (1), No. 5928.

(9) Wang, Y.; Liu, T.; Liu, J. Synergistically Boosted Degradation of Organic Dyes by CeO2 Nanoparticles with Fluoride at Low PH. *ACS Appl. Nano Mater.* **2020**, *3* (1), 842−849.

(10) Shcherbakov, A. B.; Reukov, V. V.; Yakimansky, A. V.; Krasnopeeva, E. L.; Ivanova, O. S.; Popov, A. L.; Ivanov, V. K. Ceo2 Nanoparticle-Containing Polymers for Biomedical Applications: A Review. *Polymers* **2021**, *13* (6), No. 924, DOI: 10.3390/polym13060924.

(11) Khan, M. M.; Adil, S. F.; Al-Mayouf, A. Metal Oxides as Photocatalysts. *J. Saudi Chem. Soc.* **2015**, *19* (5), 462−464.

(12) Khan, M. M.; Pradhan, D.; Sohn, Y. *Nanocomposites for Visible Light-Induced Photocatalysis*; Khan, M. M.; Pradhan, D.; Sohn, Y., Eds.; Springer Series on Polymer and Composite Materials; Springer International Publishing: Cham, 2017.

(13) Du, N.; Zhang, H.; Chen, B.; Ma, X.; Yang, D. Ligand-Free Self-Assembly of Ceria Nanocrystals into Nanorods by Oriented Attachment at Low Temperature. *J. Phys. Chem. C* **2007**, *111* (34), 12677−12680.

(14) Spezzati, G.; Fant, K.; Ahniyaz, A.; Lundin-Johnson, M.; Hensen, E. J. M.; Langermans, H.; Hofmann, J. P. Synthesis, Physicochemical Characterization, and Cytotoxicity Assessment of CeO2 Nanoparticles with Different Morphologies. *Eur. J. Inorg. Chem.* **2017**, *2017* (25), 3184−3190.

(15) Magdalane, C. M.; Kaviyarasu, K.; Vijaya, J. J.; Siddhardha, B.; Jeyaraj, B. Photocatalytic Activity of Binary Metal Oxide Nanocomposites of CeO2/CdO Nanospheres: Investigation of Optical and Antimicrobial Activity. *J. Photochem. Photobiol., B* **2016**, *163*, 77−86.

(16) Liu, D.; Tian, J.; Tang, Y.; Li, J.; Wu, S.; Yi, S.; Huang, X.; Sun, D.; Wang, H. High-Power Double-Face Flow Al-Air Battery Enabled by CeO2 Decorated MnOOH Nanorods Catalyst. *Chem. Eng. J.* **2021**, *406* (2020), No. 126772.

(17) Cheng, G.; Xiong, J.; Stadler, F. J. A Facile Polyol-Mediated Approach to Tunable CeO2Microcrystals and Their Photocatalytic Activity. *Powder Technol.* **2013**, *249*, 89−94.

(18) Xin, Y.; Yang, X.; Jiang, P.; Zhang, Z.; Wang, Z.; Zhang, Y. Synthesis of CeO2-Based Quantum Dots through a Polyol-Hydrolysis Method for Fuel-Borne Catalysts. *ChemCatChem.* **2011**, *3* (11), 1772−1778.

(19) Herricks, T.; Chen, J.; Xia, Y. Polyol Synthesis of Platinum Nanoparticles: Control of Morphology with Sodium Nitrate. *Nano Lett.* **2004**, *4* (12), 2367−2371.

(20) Matussin, S. N.; Rahman, A.; Khan, M. M. Role of Anions in the Synthesis and Crystal Growth of Selected Semiconductors. *Front. Chem.* **2022**, *10*, No. 881518, DOI: 10.3389/fchem.2022.881518.

(21) Singh, K. R. B.; Nayak, V.; Sarkar, T.; Singh, R. P. Cerium Oxide Nanoparticles: Properties, Biosynthesis and Biomedical Application. *RSC Adv.* **2020**, *10*, 27194−27214, DOI: 10.1039/D0RA04736H.

(22) Jan, H.; Khan, M. A.; Usman, H.; Shah, M.; Ansir, R.; Faisal, S.; Ullah, N.; Rahman, L. TheAquilegia Pubiflora(Himalayan Columbine) Mediated Synthesis of Nanoceria for Diverse Biomedical Applications. *RSC Adv.* **2020**, *10* (33), 19219−19231.

(23) Prasad, A. R.; Basheer, S. M.; Williams, L.; Joseph, A. Highly Selective Inhibition of *α*-Glucosidase by Green Synthesised ZnO Nanoparticles - In-Vitro Screening and in-Silico Docking Studies. *Int. J. Biol. Macromol.* **2019**, *139*, 712−718.

(24) Alqahtani, A. S.; Hidayathulla, S.; Rehman, M. T.; Elgamal, A. A.; Al-Massarani, S.; Razmovski-Naumovski, V.; Alqahtani, M. S.; el Dib, R. A.; Alajmi, M. F. Alpha-Amylase and Alpha-Glucosidase Enzyme Inhibition and Antioxidant Potential of 3-Oxolupenal and Katononic Acid Isolated from Nuxia Oppositifolia. *Biomolecules* **2020**, *10* (1), No. 61.

(25) Kajaria, D.; Tiwari, S.; Tripathi, J.; Tripathi, Y.; Ranjana. In-Vitro *α* Amylase and Glycosidase Inhibitory Effect of Ethanolic Extract of Antiasthmatic Drug - Shirishadi. *J. Adv. Pharm. Technol. Res.* **2013**, *4* (4), 206.

(26) Assefa, S. T.; Yang, E. Y.; Chae, S. Y.; Song, M.; Lee, J.; Cho, M. C.; Jang, S. Alpha Glucosidase Inhibitory Activities of Plants with Focus on Common Vegetables. *Plants* **2020**, *9* (1), 1−16.

(27) Asok, A.; Ghosh, S.; More, P. A.; Chopade, B. A.; Gandhi, M. N.; Kulkarni, A. R. Surface Defect Rich ZnO Quantum Dots as Antioxidants Inhibiting *α*-Amylase and *α*-Glucosidase: A Potential Anti-Diabetic Nanomedicine. *J. Mater. Chem. B* **2015**, *3* (22), 4597−4606.

(28) Matussin, S. N.; Khan, F.; Chandika, P.; Harunsani, M. H.; Ahmad, N.; Kim, Y. M.; Jung, W. K.; Khan, M. M. Effects of NO3−, Cl−, and CH3COO− Anions and Diethylene Glycol on the Morphological, Structural, Antidiabetic, and Cell Viability Properties of CeO2 Nanoparticles. *RSC Adv.* **2023**, *13* (23), 15421−15436.

(29) Badeggi, U. M.; Badmus, J. A.; Botha, S. S.; Ismail, E.; Marnewick, J. L.; Africa, C. W. J.; Hussein, A. A. Biosynthesis, Characterization, and Biological Activities of Procyanidin Capped Silver Nanoparticles. *J. Funct Biomater* **2020**, *11* (3), No. 66.

(30) Khan, M. A. M.; Khan, W.; Ahamed, M.; Alhazaa, A. N. Microstructural Properties and Enhanced Photocatalytic Performance of Zn Doped CeO2 Nanocrystals. *Sci. Rep* **2017**, *7* (1), No. 12560.

(31) Nosrati, H.; Sarraf-Mamoory, R.; Canillas Perez, M.; Le, D. Q. S.; Zolfaghari Emameh, R.; Bünger, C. E. Characteristics of Hydroxyapatite-Reduced Graphene Oxide Composite Powders Synthesized via Hydrothermal Method in the Absence and Presence of Diethylene Glycol. *Open Ceram.* **2021**, *5*, 100067 DOI: 10.1016/j.oceram.2021.100067.

(32) Gondolini, A.; Mercadelli, E.; Sanson, A.; Albonetti, S.; Doubova, L.; Boldrini, S. Effects of the Microwave Heating on the Properties of Gadolinium-Doped Cerium Oxide Prepared by Polyol Method. *J. Eur. Ceram. Soc.* **2013**, *33* (1), 67−77.

(33) He, L.; Ren, Y.; Fu, Y.; Yue, B.; Edman Tsang, S. C.; He, H. Morphology-Dependent Catalytic Activity of Ru/CeO2 in Dry Reforming of Methane. *Molecules* **2019**, *24* (3), No. 526, DOI: 10.3390/molecules24030526.

(34) Matussin, S. N.; Khan, F.; Harunsani, M. H.; Kim, Y.-M.; Khan, M. M. Effect of Pd-Doping Concentrations on the Photocatalytic, Photoelectrochemical, and Photoantibacterial Properties of CeO2. *Catalysts* **2023**, *13* (1), 96.

(35) Tou, M.; Michalsky, R.; Steinfeld, A. Solar-Driven Thermochemical Splitting of CO2 and In Situ Separation of CO and O2 across a Ceria Redox Membrane Reactor. *Joule* **2017**, *1* (1), 146−154.

(36) Chen, G.; Guo, M. Rapid Screening for *α*-Glucosidase Inhibitors from Gymnema Sylvestre by Affinity Ultrafiltration−HPLC-MS. *Front Pharmacol* **2017**, *8*, No. 228, DOI: 10.3389/fphar.2017.00228.

(37) Khan, K. M.; Rahim, F.; Wadood, A.; Kosar, N.; Taha, M.; Lalani, S.; Khan, A.; Fakhri, M. I.; Junaid, M.; Rehman, W.; Khan, M.; Perveen, S.; Sajid, M.; Choudhary, M. I. Synthesis and Molecular Docking Studies of Potent *α*-Glucosidase Inhibitors Based on Biscoumarin Skeleton. *Eur. J. Med. Chem.* **2014**, *81*, 245−252.

(38) Alqahtani, A. S.; Hidayathulla, S.; Rehman, T.; Elgamal, A. A.; Dib, R. A.; El; Alajmi, M. F. Biomolecules-10-00061.Pdf.

(39) Shao, T.; Yuan, P.; Zhu, L.; Xu, H.; Li, X.; He, S.; Li, P.; Wang, G.; Chen, K. Carbon Nanoparticles Inhibit *α*-Glucosidase Activity and Induce a Hypoglycemic Effect in Diabetic Mice. *Molecules* **2019**, *24* (18), No. 3257.

(40) Zhang, M.; Wang, H.; Wang, B.; Ma, Y.; Huang, H.; Liu, Y.; Shao, M.; Yao, B.; Kang, Z. Maltase Decorated by Chiral Carbon Dots with Inhibited Enzyme Activity for Glucose Level Control. *Small* **2019**, *15* (48), 1−7.

(41) Kong, B.; Seog, J. H.; Graham, L. M.; Lee, S. B. Experimental Considerations on the Cytotoxicity of Nanoparticles. *Nanomedicine* **2011**, *6*, 929−941.

(42) Akter, M.; Sikder, Md. T.; Rahman, Md. M.; Ullah, A. K. M. A.; Hossain, K. F. B.; Banik, S.; Hosokawa, T.; Saito, T.; Kurasaki, M. A Systematic Review on Silver Nanoparticles-Induced Cytotoxicity: Physicochemical Properties and Perspectives. *J. Adv. Res.* **2018**, *9*, 1−16.

(43) Lewinski, N.; Colvin, V.; Drezek, R. Cytotoxicity of Nanoparticles. *Small* **2008**, *4* (1), 26−49.

(44) Nan, A.; Bai, X.; Son, S. J.; Lee, S. B.; Ghandehari, H. Cellular Uptake and Cytotoxicity of Silica Nanotubes. *Nano Lett.* **2008**, *8* (8), 2150−2154.